

Joint Estimation of Hemodynamic Response Function and Voxel Activation in functional MRI Data

Priya Aggarwal¹, Anubha Gupta¹, and Ajay Garg²

¹ Department of Electronics and Communication Engineering, IIIT-Delhi, India

² Department of Neuroradiology, Neurosciences Centre, AIIMS, Delhi, India
priyaa@iiitd.ac.in, anubha@iiitd.ac.in, drajaygarg@gmail.com

Abstract. *This paper proposes a method of voxel-wise hemodynamic response function (HRF) estimation using sparsity and smoothing constraints on the HRF. The slow varying baseline drift at the voxel time-series is initially estimated via empirical mode decomposition (EMD). This estimation is refined by two-stage optimization that estimates HRF and slow-varying noise iteratively. In addition, this paper proposes a novel method of finding voxel activation via projection of voxel time-series on signal subspace constructed using the prior estimates of HRF. The performance of the proposed method is demonstrated on both synthetic and real fMRI data.*

Keywords- *functional MRI, Hemodynamic Response Function, Activation detection.*

1 Introduction

Blood oxygen-level dependent (BOLD) functional magnetic resonance imaging (fMRI) is a non-invasive method to analyze human brain activity under different tasks such as visual, hearing, cognitive, etc [1]. It relates the neural activity with the temporal impulse response which is known as hemodynamic response function (HRF). In this manner, HRF is a proxy measure of underlying neuronal activity in brain. HRF not only varies across multiple subjects, but also in different regions of the brain of a single subject. HRF estimation can play a crucial role in estimating brain voxels activity accurately.

In the literature, HRF estimation has been done by two approaches: via region-based approach and via voxel-based approach [2]. In the region-based approach, regions of interest (ROIs) are extracted by either assuming equally sized regions [3] or via parcellation algorithm [4]. It is assumed that the HRF is same in all the voxels of a region. Hence, the mean of fMRI signal in the ROI is considered for HRF estimation. But, in actual scenario, some voxels may have different HRF within that ROI. Thus, estimated HRF may be suboptimal. In order to overcome the above shortcoming, various methods of voxel-based HRF estimation have been proposed in the literature [5-6]. Here, HRF is assumed to vary across different voxels. However, due to poor signal-to-noise ratio of fMRI time series, HRF estimates may be potentially misleading. Smoothing in the pre-processing stage can overcome this problem.

In addition to the above classification, there are parametric and nonparametric methods of HRF estimation. In the parametric methods, shape of HRF is assumed to be known apriori. However, single nonlinear function is not accurate to model HRFs across the entire brain. Nonparametric methods of HRF estimation do not restrict the shape of HRF and estimate HRF at each time point [5]. In [5], general linear model (GLM) is applied on each voxel to characterize voxel activity via best linear combination of the predictors [5]. The nonparametric method in [6] imposes sparsity constraint on HRF in time-domain. However, sparsity of HRF may be better modeled in the wavelet-domain as compared to the time-domain. In order to account for HRF variability across ROI, this paper considers voxel-based nonparametric approach for HRF estimation. Our method does not require priors on the parameters of HRF. A consistent voxel-wise HRF estimation along with sparsity and smoothing constraint is proposed in this paper. Additionally, estimated HRFs in a region are used to form signal subspace and projection of voxel time-series onto this signal subspace is used for robust detection of active *seed* voxel in the ROI.

This paper is organized as follows. Section 2 describes the fMRI time series model. Section 3 describes the proposed HRF estimation method. This section also presents the proposed method of voxel activation detection via subspace modeling. Simulation results on both simulated and real fMRI data are presented in Section 4. In the end, conclusions are presented in section 5.

Notations: We use lower case bold letters for vectors, upper case bold letters for matrices, and lower case italics letters for scalars.

2 Preliminaries

This section presents a brief background on fMRI signal time series and EMD.

2.1 Cerebral Hemodynamic Response Function

The BOLD fMRI signal is captured via T_2^* weighted imaging via MR scanner. Let us consider that M no. of brain volumes, at time instants t_j where $j = 1, 2, \dots, M$ have been captured during an fMRI experiment. The intensity of a particular voxel V_i in the scanned brain volumes can be represented as a time-series $\mathbf{y}_i = [y_{i,1}, y_{i,2}, \dots, y_{i,M}]$. This signal characterizes the BOLD time-series or signal at a particular voxel in brain.

In general, an fMRI signal is comprised of a) an activity-induced signal modeled as convolution of stimulus function with HRF of that region, b) a slow varying noise component, also called as baseline drift, and c) noise that is generally assumed to be additive white Gaussian noise (AWGN) for the sake of simplicity [6]. In other words, we can write

$$\mathbf{y}_i = \mathbf{S}\mathbf{h}_i + \mathbf{f}_i + \xi_i. \quad (1)$$

where \mathbf{S} is $M \times L$ convolution matrix consisting of known lagged stimulus covariates. \mathbf{S} depends on experimental design and is independent of voxel position. \mathbf{h}_i is the amplitude of L -length HRF at voxel V_i , \mathbf{f}_i is the M -time point baseline drift

at voxel V_i , and ξ_i is the vector of M -length AWGN with $\xi_i \in N(0, \sigma^2 \mathbf{I})$. This model does not assume any apriori shape of HRF. The baseline drift represented by $\mathbf{f}_i = [f_{i,1}, f_{i,2}, \dots, f_{i,M}]$ is assumed to be independent of the experimental design matrix \mathbf{S} . This is to note that, in general, experimental paradigms in fMRI are constructed with single stimulus paradigm as considered in this paper to determine activated regions to build functional connectivity maps. However, the framework can be extended to multiple stimulus (say two) as below:

$$\mathbf{y}_i = \alpha_1 \mathbf{S}_1 \mathbf{h}_i + \alpha_2 \mathbf{S}_2 \mathbf{h}_i + \mathbf{f}_i + \xi_i. \quad (2)$$

where \mathbf{S}_1 and \mathbf{S}_2 are two different stimuli and α_1 and α_2 are the associated constants. However, for this framework, fMRI experiment data has to be captured for two different stimuli one by one in different time slots in the same session.

2.2 Empirical Mode Decomposition

Empirical mode decomposition (EMD) is an adaptive data driven approach that decomposes any nonlinear and non-stationary signal such as biomedical signals into amplitude and frequency modulated (AM-FM) components [7]. These functions are also called as intrinsic mode functions (IMFs) [7]. These IMFs are linearly independent of each other and capture the oscillations (or modes) that are intrinsically part of the given signal [7]. In general, the estimated IMFs are in the order of decreasing frequency. Thus, the first IMF corresponds to the high frequency oscillations, while the last IMF has the slow varying component. In general, signal $f[n]$ can be represented using IMFs as below:

$$f[n] = \sum_{k=1}^Q d_k[n] + r_Q[n] \quad (3)$$

where Q = total number of IMFs, $d_k[n]$ for $k = 1, \dots, Q$ are the IMFs, $r_Q[n]$ is the last IMF, and stopping criterion defined in the EMD algorithm terminates the iterative procedure providing all IMFs. Currently, this method is being applied in various applications including biomedical, geological time-series analysis, etc. [7, 8].

3 Proposed Estimation of HRF and Voxel Activation

3.1 Proposed HRF Estimation Method

The time-series at a voxel V_i is represented as given in (1). In this equation, there are two unknowns: the HRF \mathbf{h}_i and the slow varying baseline drift \mathbf{f}_i . In the literature, the theoretical shape of the HRF is assumed to be the one shown in Fig. 1(a) [3].

From Fig. 1(a), we draw the following assumptions on HRF:

- A1) HRF is a smooth function over time. Thus, we can apply the Tikhonov regularisation technique for incorporating a smoothness constraint on the

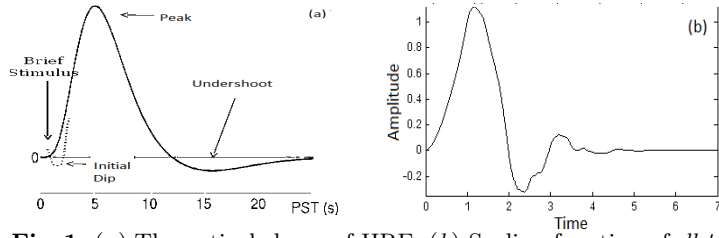


Fig. 1. (a):Theoretical shape of HRF; (b) Scaling function of *db4*

HRF [4]. This implies that the minimization of l^2 norm of $\mathbf{D}\mathbf{h}_i$ can be used as a constraint, where \mathbf{D} is the second difference matrix operator given as:

$$\mathbf{D} = \begin{bmatrix} 2 & -1 & 0 & \dots & 0 & 0 & 0 \\ -1 & 2 & -1 & 0 & \dots & 0 & 0 \\ 0 & -1 & 2 & -1 & 0 & \dots & \dots \\ 0 & 0 & \dots & \dots & 2 & -1 & 0 \\ \dots & \dots & \dots & \dots & -1 & 2 & -1 \\ 0 & 0 & \dots & 0 & 0 & -1 & 2 \end{bmatrix}$$

A2) Refer to Fig. 1(b) that shows the shape of the scaling function corresponding to the orthogonal wavelet *Daubechies-4* (or *db4*). This shape is very similar to the theoretical HRF shape shown in Fig. 1(a). From these two figures, it is obvious that if HRF is analyzed via *db4*, it will be sparse in the wavelet domain. Thus, we assume that $\mathbf{W}\mathbf{h}_i$ is sparse, where \mathbf{W} is the matrix operator corresponding to *db4*.

Using the above assumptions, we formulate the problem of HRF estimation, mathematically, using Lagrangian multiplier method as below:

$$\hat{\mathbf{h}}_i = \underset{h_i}{\operatorname{argmin}} \|\mathbf{y}_i - \mathbf{S}\mathbf{h}_i - \mathbf{f}_i\|_2 + \lambda_1 \|\mathbf{D}\mathbf{h}_i\|_2 + \lambda_2 \|\mathbf{W}\mathbf{h}_i\|_1 + \lambda_3 \|\mathbf{f}_i\|_2 \quad (4)$$

where λ_1 , λ_2 , and λ_3 are the Lagrangian multipliers or regularization parameters. In (4), baseline drift is also unknown. In order to solve this problem, we carry out optimization in two stages, wherein we solve for $\hat{\mathbf{h}}_i$ and $\hat{\mathbf{f}}_i$ iteratively with the first iteration estimate $\hat{\mathbf{f}}_i^{(1)}$ drawn as the last IMF of EMD decomposition. The pseudo code for the estimation of $\hat{\mathbf{h}}_i$ is provided in Table-1. This is to note that optimization is carried out in CVX, a package for specifying and solving convex programs [8].

3.2 Proposed Voxel Activation Detection via Subspace Modeling

In order to estimate voxel activation, we formulate the following strategy. First, we estimate HRF at N no. of voxels with significant magnitude in the activity sensitive region using *Algorithm-1*. Within a region, the shape of HRF is somewhat similar, hence, we construct the signal subspace using estimated HRFs in that region. To this end, we use the projection operator based approach. First, we convolve each of these N no. of HRFs with the stimulus function $s(n)$ of length M (no. of brain scan volumes) as below:

$$\mathbf{x}_i = x_i[n] = s[n] \otimes h_i[n] = \sum_{k=0}^{L-1} h_i[k]s[n-k] \quad (5)$$

Table-1

Algorithm-1: Pseudo Code for Estimation of $\hat{\mathbf{h}}_i$

Input Parameters	Tikhonov regularisation matrix \mathbf{D} (size $L \times L$) Daubechies-4 matrix \mathbf{W} (size $L \times L$) Stimulus or Design matrix \mathbf{S} (size $M \times L$) Lagrangian multipliers λ_1, λ_2 , and λ_3 (scalars)
Input Data	Measured voxel V_i 's time series stacked in a column \mathbf{r}_i (size $M \times 1$)
Start	
<i>Step-1</i>	$\mathbf{y}_i = \text{detrond}(\mathbf{r}_i)$
<i>Step-2</i>	Carry out EMD decomposition of \mathbf{y}_i and initialize $\hat{\mathbf{f}}_i^{(1)} = \text{Last IMF}$.
<i>Step-3</i>	Compute first estimate of HRF $\hat{\mathbf{h}}_i^{(1)}$ $\hat{\mathbf{h}}_i^{(1)} = \arg \min_{\mathbf{h}_i} \left\ \mathbf{y}_i - \mathbf{S}\mathbf{h}_i - \hat{\mathbf{f}}_i^{(1)} \right\ _2 + \lambda_1 \left\ \mathbf{D}\mathbf{h}_i \right\ _2 + \lambda_2 \left\ \mathbf{W}\mathbf{h}_i \right\ _1$
<i>Step-4</i>	do $\hat{\mathbf{f}}_i^{(k+1)} = \arg \min_{\mathbf{f}_i} \left\ \mathbf{y}_i - \mathbf{S}\hat{\mathbf{h}}_i^{(k)} - \mathbf{f}_i \right\ _2 + \lambda_3 \left\ \mathbf{f}_i \right\ _2$ $\hat{\mathbf{h}}_i^{(k+1)} = \arg \min_{\mathbf{h}_i} \left\ \mathbf{y}_i - \mathbf{S}\mathbf{h}_i - \hat{\mathbf{f}}_i^{(k)} \right\ _2 + \lambda_1 \left\ \mathbf{D}\mathbf{h}_i \right\ _2 + \lambda_2 \left\ \mathbf{W}\mathbf{h}_i \right\ _1$ while $\hat{\mathbf{h}}_i^{(k+1)} \neq \hat{\mathbf{h}}_i^{(k)}$ and $\hat{\mathbf{f}}_i^{(k+1)} \neq \hat{\mathbf{f}}_i^{(k)}$
Output	$\hat{\mathbf{h}}_i^{(k)}$

where $n = 0, 1, \dots, M-1$ and $i = 0, 1, \dots, N-1$. Next, we assume that these N no. of vectors \mathbf{x}_i form the basis vectors of signal subspace χ and stack these into the columns of matrix \mathbf{X} of size $(M \times N)$. We compute the projection matrix (operator) \mathbf{P}_X corresponding to the signal subspace χ as below [9]:

$$\mathbf{P}_X = \mathbf{X}(\mathbf{X}^T \mathbf{X})^{-1} \mathbf{X}^T \quad (6)$$

where \mathbf{P}_X is a symmetric and idempotent projection matrix. Since this signal subspace has been constructed from the estimated HRFs of the voxels with significant magnitude, this space will not be influenced largely with AWGN noise and the baseline drift. Now, this projection matrix \mathbf{P}_X is used to project a detrended voxel time series \mathbf{y}_k onto signal subspace χ as below:

$$\mathbf{w}_k = \mathbf{P}_X \mathbf{y}_k \quad (7)$$

for $k = 0, 1, \dots, p-1$ where p corresponds to the no. of voxels in the activity-sensitive region of the brain. The norm of vectors \mathbf{w}_k are computed for all p voxels. The voxel with the highest norm is labeled as the *seed* voxel of this region. This approach will take care of any inhomogeneity left in the neighborhood even after motion correction, removal of drift noise, etc. that might confound seed voxel. Voxels with norm greater than the threshold γ are declared as active voxels, i.e.,

$$\text{Declare } V_k = \text{active if } \text{norm}(\mathbf{w}_k) > \gamma \quad (8)$$

4 Validation of the Proposed Method

In this section, we test the proposed joint method of HRF estimation and activation detection on the synthetic and real fMRI data.

4.1 Results on Synthetic fMRI Data

We generated a synthetic fMRI time series by convolving the stimulus function with the canonical HRF. Our canonical HRF of length $L=20$ is constructed using the difference of two gamma functions [4]. The plot of HRF $h[n]$ is shown in Fig. 2(a). We generated 200 time points of the synthetic BOLD fMRI signal as below:

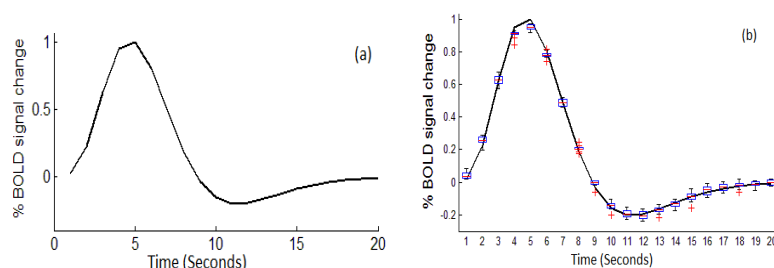


Fig. 2. (a): Synthetic HRF $h[n]$; (b) Estimated HRF \hat{h}_i using *Algorithm-1*

$$\mathbf{y} \equiv y[n] = s[n] \otimes h[n] + \xi[n] \quad (9)$$

Since we used real data with block-stimulus experiment design, we generated synthetic data with the same experimental paradigm. In the block experiment, block of 60s is generated with 30s on and 30s off time. Additive white Gaussian noise is generated with variances 0.75, 0.5, 0.25, 0.1, and 0.05. For computing the mean square error (MSE), 500 Monte Carlo cycles have been performed over voxel time-series (i.e., considering 500 different realizations of noise time-series). MSE between the canonical and estimated HRF is calculated as below:

$$MSE = \frac{1}{500} \sum_{k=1}^{500} \left[\frac{1}{L} \sum_{n=0}^{L-1} (\hat{h}_k[n] - h_k[n])^2 \right] \quad (10)$$

Since we did not corrupt the synthetic data with the slow varying baseline drift, only HRF was required to be estimated using *Algorithm-1*. The estimated HRF for noise variance $\sigma^2 = 0.1$ and with regularization parameters of $\lambda_1 = 1$ and $\lambda_2 = 0.2$ (determined empirically) is shown in Fig. 2(b).

Table-2: MSE calculated between estimated and canonical (assumed) HRF

	Noise Variance σ^2				
	0.05	0.1	0.25	0.5	0.75
Method of [6]	0.0522	0.0839	0.1689	0.3405	0.6474
Proposed	0.0153	0.0186	0.0374	0.0744	0.1012
Proposed without smoothing	0.0179	0.0361	0.0697	0.1253	0.2406

The results of proposed algorithm are compared with the method of [6] and tabulated in Table-2. In [6], sparsity on HRF is imposed in the time-domain, while based on the shape and our discussion in Section 3.1, we find it more appropriate to consider sparsity of HRF in the wavelet-domain. In addition, we have imposed smoothness constraint on HRF that was not imposed in [6]. From Table-2, we observe that the proposed method with both smoothing and wavelet-domain sparsity constraint outperforms [6].

4.2 Results on Real fMRI Data

For testing the proposed framework on real fMRI data, we utilized the block design paradigm based auditory fMRI dataset available at SPM website [10]. This auditory dataset consists of acquisitions of 64 contiguous slices with $64 \times 64 \times 64$ voxels of voxel size $3 \times 3 \times 3 \text{ mm}^3$. It contains 96 time points (or 96 acquisitions) with repetition time of 7s. Pre-processing of this data has been carried out using SPM8 toolbox with the procedure as outlined specifically for this dataset in Chapter 28 of SPM8 manual [10]. Pre-processing steps include realignment (with the first scan for removal of motion artefact), co-registration (with the mean fMRI scan generated in the step of realignment), normalisation (with the MNI atlas), and smoothing (using a 6mm full width at half maximum (FWHM) Gaussian kernel). These steps provided 96 brain volumes of $79 \times 95 \times 68$ voxels each. First 12 scans were discarded, resulting in 84 brain volumes. Subject was given stimulus starting with the condition of rest, auditory, rest, and so on.

In general, Brodmann regions 22, 40, 41 are found to be associated with the auditory stimulus. We have tested the proposed methodology on Brodmann region 22. We extracted this ROI (Z) using *WFU Pickatlas Tool* [11]. Total 1720 voxels were extracted from this ROI. Next, we estimated HRF at 10 voxels with the highest norm, out of which 2 HRFs are shown in Fig. 3(a). The regularization parameters of $\lambda_1 = 1$, $\lambda_2 = 0.2$ (same as used for synthetic data) and $\lambda_3 = 0.1$ were used in the optimization routine for HRF estimation.

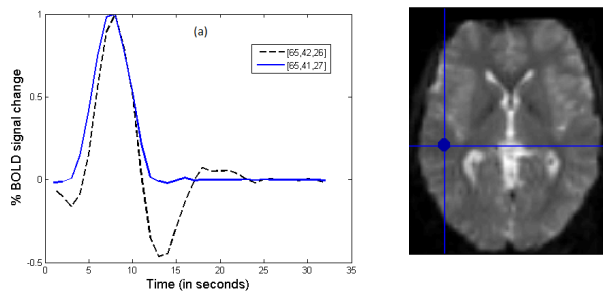


Fig. 3. (a): Estimated HRF estimated using *Algorithm-1* on voxel positions ([65,41,27]-solid line; [65,42,26]-dotted line); (b) Active Seed Voxel [65,42,25]

Next, we constructed the projection operator using the estimated HRFs at 30 highest norm voxels as discussed in Section 3.2, projected the de-trended

time-series \mathbf{y}_k of all the voxels p of region Z using (7). Thereafter, we computed norm of vectors \mathbf{w}_k of all p voxels. In the end, we declare the voxel with the highest norm as the seed voxel of activity-specific region Z . The coordinates of *seed* voxel on MNI frame of reference are found to be [65,42,25], and is shown on a 10mm diameter in Fig. 3(b). The position of seed voxel was validated by the radiologist.

5 Conclusion

In this paper, we have presented a joint method of voxel-wise hemodynamic response function (HRF) estimation and voxel activation detection. We removed the slow varying baseline drift using EMD along with the constraint optimization using sparsity on HRF in the wavelet-domain and smoothness of HRF in time-domain. This estimation is refined by two-stage optimization that estimates HRF and slow-varying noise iteratively. In addition, we propose a novel method of finding active seed voxel via projection of voxels time series on signal subspace constructed using the estimates of HRF. Since the proposed framework estimates HRF voxel-wise instead of region-wise, the determination of seed voxel in a region will be more accurate.

References

1. S. Ogawa, et al., "Brain magnetic resonance imaging with contrast dependent on blood oxygenation," *PNAS USA*, vol. 87, no. 24, pp. 9868–9872, 1990.
2. G. Glover, "Deconvolution of impulse response in event related BOLD fMRI," *Neuroimage*, vol. 9, pp. 416–429, 1999.
3. S. Makni, et al., "A fully Bayesian approach to the parcel-based detection-estimation of brain activity in fMRI," *NeuroImage*, vol. 41, pp. 941–969, July 2008.
4. N. Bezargani and A. Nostratinia, "Joint maximum likelihood estimation of activation and Hemodynamic Response Function for fMRI," *Elsevier Medical Image Analysis*, vol. 18, pp. 711–724, 2014.
5. A. F. Sole et al., "Anisotropic 2-D and 3-D averaging of fMRI signals," *IEEE Trans. Med. Imag*, vol. 20, pp. 86–93, Feb. 2001.
6. A. K. Seghouane and L. A. Johnston, "Consistent hemodynamic response estimation function in fMRI using sparse prior information," *IEEE ISBI*, pp. 596–599, May 2014.
7. N. E. Huang, et al., "The empirical mode decomposition and hilbert spectrum for nonlinear and nonstationary time series analysis," *Proc. Roy. Soc. London*, pp. 454–460, 1998.
8. M. Grant and S. Boyd, "CVX: Matlab software for disciplined convex programming, version 2.0 beta. <http://cvxr.com/cvx>," September 2013.
9. S. Agarwal and A. Gupta, "Fractal and EMD based Removal of Baseline Wander and Powerline Interference from ECG Signals," *Computers in Biology and Medicine, Elsevier*, vol. 43, issue 11, pp. 1889–1899, Nov. 2013.
10. <http://www.fil.ion.ucl.ac.uk/spm/data/>
11. J. A. Maldjian, et al., "An automated method for neuroanatomic and cytoarchitectonic atlas-based interrogation of fmri data sets (WFU Pickatlas, version 3.05)," *NeuroImage*, vol. 19, pp. 1233–1239.